Experimental and theoretical studies of rate coefficients for the reaction O (P 3) + C H 3 O H at high temperatures

Chih-Wei Lu, Shen-Long Chou, Yuan-Pern Lee, Shucheng Xu, Z. F. Xu, and M. C. Lin

Citation: The Journal of Chemical Physics **122**, 244314 (2005); doi: 10.1063/1.1924390
View online: http://dx.doi.org/10.1063/1.1924390
View Table of Contents: http://scitation.aip.org/content/aip/journal/jcp/122/24?ver=pdfcov
Published by the AIP Publishing

Experimental and theoretical studies of rate coefficients for the reaction $O(^3P)+CH_3OH$ at high temperatures

Chih-Wei Lu and Shen-Long Chou
Department of Chemistry, National Tsing Hua University, 101, Section 2, Kuang Fu Road, Hsinchu 30013, Taiwan

Yuan-Pern Lee[a),b)]
Department of Applied Chemistry and Institute of Molecular Science, National Chiao Tung University, 1001, Ta Hsueh Road, Hsinchu 30010, Taiwan and Institute of Atomic and Molecular Sciences, Academia Sinica, Taipei 106, Taiwan

Shucheng Xu, Z. F. Xu, and M. C. Lin[a),c)]
Department of Chemistry, Emory University, Atlanta, Georgia 30322

(Received 1 February 2005; accepted 29 March 2005; published online 29 June 2005)

Rate coefficients of the reaction $O(^3P)+CH_3OH$ in the temperature range of 835–1777 K were determined using a diaphragmless shock tube. O atoms were generated by photolysis of SO_2 with a KrF excimer laser at 248 nm or an ArF excimer laser at 193 nm; their concentrations were monitored via atomic resonance absorption excited by emission from a microwave-discharged mixture of O_2 and He. The rate coefficients determined for the temperature range can be represented by the Arrhenius equation, $k(T)=(2.29\pm0.18)\times10^{-10}\exp[-(4210\pm100)/T]$ cm^3 molecule^{-1} s^{-1}; unless otherwise noted, all the listed errors represent one standard deviation in fitting. Combination of these and previous data at lower temperature shows a non-Arrhenius behavior described as the three-parameter equation, $k(T)=(2.74\pm0.07)\times10^{-18}T^{2.25\pm0.13}\exp[-(1500\pm90)/T]$ cm^3 molecule^{-1} s^{-1}. Theoretical calculations at the Becke-3-Lee–Yang–Parr (B3LYP)/6–311+$G(3df,2p)$ level locate three transition states. Based on the energies computed with coupled clusters singles, doubles (triples) [CCSD(T)]/6–311+$G(3df,2p)$//B3LYP/6–311+$G(3df,2p)$, the rate coefficients predicted with canonical variational transition state theory with small curvature tunneling corrections agree satisfactorily with the experimental observations. The branching ratios of two accessible reaction channels forming $OH+CH_2OH$ (1a) and $OH+CH_3O$ (1b) are predicted to vary strongly with temperature. At 300 K, reaction (1a) dominates, whereas reaction (1b) becomes more important than reaction (1a) above 1700 K. © *2005 American Institute of Physics*. [DOI: 10.1063/1.1924390]

I. INTRODUCTION

Methanol (CH_3OH) is considered as an important alternative fuel; it may be used directly in an internal engine via combustion or in a fuel cell via catalytic electrolytic reactions. The reaction

$$O(^3P)+CH_3OH\rightarrow OH+CH_2OH \quad (1a)$$

$$\rightarrow OH+CH_3O \quad (1b)$$

$$\rightarrow HO_2+CH_3 \quad (1c)$$

with three energetically accessible channels is one of the most important processes in combustion of CH_3OH. The branching between these channels plays an important role in the formation of the end products, inhibition of flames, and formation of soot.[1]

The rate coefficients of reaction (1) have been determined in the temperature range of 273–1006 K by several groups.[2–9] The experimental conditions, reported rate coefficients near room temperature, and Arrhenius parameters of these studies are listed in Table I for comparison; the corresponding Arrhenius plots are also shown in Fig. 1. Most rate coefficients are reported to be within a factor of two except those of LeFevre *et al.*[2] (designated LMT) and Basevich *et al.*[3] (designated BKF) which are 4–17 times greater near 298 K, and those of Avramenko *et al.*[8] (designated AKK) which are about three times smaller. The rate coefficients of this reaction show a non-Arrhenius behavior, as the reported activation energies increases with the temperature of measurements. The two measurements covering limited temperature range below 450 K by LMT (Ref. 2) and by Owens and Roscoe[4] (designated OR) have activation energies (E_a/R =1150 and 1540 K, respectively) smaller than the two reports of $E_a/R\cong2640\pm110$ K by Keil *et al.*[5] (designated KTSKM) and Grotheer and Just[6] (designated GJ) covering temperatures up to ~1000 K. The experiments in the inter-

[a)]Authors to whom correspondence should be addressed.
[b)]FAX: 886-3-5713491. Electronic mail: yplee@mail.nctu.edu.tw
[c)]Also at National Science Council Distinguished Visiting Professor at the Center for Interdisciplinary Molecular Science, National Chiao Tung University, Taiwan. FAX: 1-404-727-6586. Electronic mail: chemmcl@emory.edu

TABLE I. Summary of reported experimental rate coefficients using various methods.

Temperature (K)	Pressure (gas) (Torr)	$k(\sim 298\ \mathrm{K})$ (10^{-15})[a]	A (10^{-12})[a]	E_a/R (K)	Method[b]	Reference
347–506			0.85	1560	DF/PCA	Avramenko *et al.* (AKK) (Ref. 8)
273–438	1.48–2.41 (O_2,He)	51.5±5.8	2.82±1.10	1147±101	DF/ESR	LeFevre *et al.* (LMT) (Ref. 2)
300–830		232	7.11	1020	DF/ESR	Basevich *et al.* (BKF) (Ref. 3)
301–451	1.00–1.76 (N_2,NO)	13.6±0.83	2.41±0.01	1540±144	DF/CL and MS	Owens and Roscoe (OR) (Ref. 4)
298	9.25 (Ar)	0.0598			FP/RF	Lalo and Vermeil (LV) (Ref. 9)
298–998	2.15–4.41 (O_2,He)	5.82±0.54	27.0±5.0	2530±80	DF/RF	Keil *et al.* (KTSKM) (Ref. 5)
329–527	50–400 (Ar), 100–200 (Ar:N_2=9:1)				FP/RF	
300–1006			57.0±19.0	2750±150	DF/TOF	Grotheer and Just (GJ) (Ref. 6)
297–544	27.2–45.9 (NO,NO_2)	8.28±0.623	16.3±4.5	2267±111	PM/CL	Failes *et al.* (FSPI) (Ref. 7)
835–1777	1086–1953 (Ar)		229±18[c]	4210±100[c]	ST/ABS	This work[c]

[a]In units of $\mathrm{cm^3\ molecule^{-1}\ s^{-1}}$.
[b]DF: discharge flow; FP: flash photolysis; PM: phase modulation; ST: shock tube; PCA: product collection and analysis; ESR: electron-spin resonance; CL: chemiluminescence; MS: mass spectrometry; RF: resonance fluorescence; TOF: time-of-flight mass; ABS: absorption.
[c]$k(T)=(2.74\pm0.07)\times10^{-18}T^{2.25\pm0.13}\exp[-(1500\pm90)/T]\ \mathrm{cm^3\ molecule^{-1}\ s^{-1}}$ for a combined fit of the data from KTSKM and this work.

mediate temperature range of 297–544 K by Failes *et al.*[7] (designated FSPI) yield an intermediate value of $E_a/R = 2270\pm110$ K.

Although the two sets of experiments by KTSKM (Ref. 5) and GJ (Ref. 6) at high temperatures show similar values of E_a/R (2530±80 and 2750±150 K, respectively), rate coefficients vary by as much as 1.7 times at 1000 K partly because of variations in the Arrhenius preexponential factors (2.7×10^{-11} and $5.7\times10^{-11}\ \mathrm{cm^3\ molecule^{-1}\ s^{-1}}$, respectively).[5,6] The experimental data are lacking for temperatures above 1006 K.

To the best of our knowledge, there have been no high-level quantum-chemical calculations performed for the O $+CH_3OH$ system. Tsang[10] combined the existing experimental data with a transition state theory using bond-energy-bond-order (BEBO) approximations and predicted the temperature dependence of the rate coefficient to be

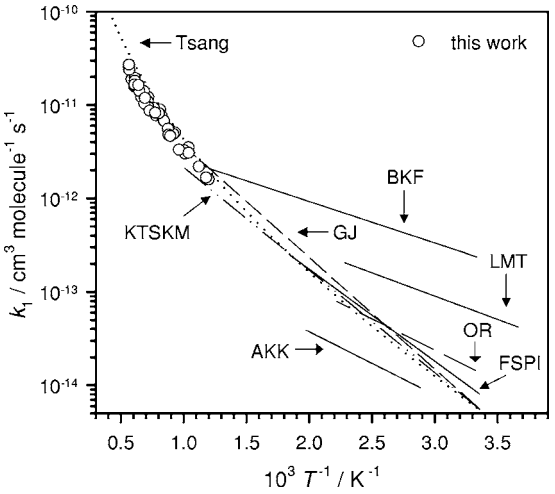

FIG. 1. Arrhenius plots of k_1 for the reaction O+CH_3OH. Our data are shown as symbols ○. Previous results are shown as lines of various types drawn for the temperature range of study. A combination of first character of each author's last name is used to indicate previous reports, as listed in Table I.

$$k_1 = 6.44\times10^{-19}T^{2.50}\times\exp[-(1550/T)]\ \mathrm{cm^3\ molecule^{-1}\ s^{-1}}. \quad (2)$$

The rate coefficient is predicted to increase rapidly at temperatures above 1000 K, yielding an upward curved Arrhenius plot.

Because of the importance of this reaction in combustion, kinetic data at higher temperatures are needed. We have determined the rate coefficients of the title reaction up to 1777 K with a diaphragmless shock tube. We also performed the theoretical calculations on this reaction to compare with our experimental measurements and to understand the competition between the two channels at varied temperatures.

II. EXPERIMENTS

The details of the diaphragmless shock tube apparatus have been described previously.[11,12] The shock tube (length of 5.9 m and inside diameter (i.d.) of 7.6 cm) is coupled to a detection system using atomic resonance absorption. The speed of the shock wave was determined with pressure sensors and time-frequency counters. A microwave-discharged lamp with a flowing gas mixture of ~1% O_2 in He served as a light source for atomic absorption of O atoms. Emission at 130.23, 130.49, and 130.60 nm, corresponding to atomic transitions of $O(^3S-{}^3P_{2,1,0})$, passes perpendicularly near the end of the shock tube and a vacuum UV monochromator (reciprocal linear dispersion of 4.0 nm $\mathrm{mm^{-1}}$ and slit width of 350 μm) before being detected with a solar-blind photomultiplier tube (PMT). Variation of the signal from the PMT was monitored with a digital storage oscilloscope and transferred to a computer for further processing.

For kinetic measurements, O atoms were generated from laser photolysis of SO_2 at 248 or 193 nm. At 248 nm, absorption cross section of SO_2 is $7.7\times10^{-20}\ \mathrm{cm^2}$ at 1100 K and $5.3\times10^{-19}\ \mathrm{cm^2}$ at 2000 K.[13] At 193 nm, absorption cross section of SO_2 is $3.4\times10^{-18}\ \mathrm{cm^2}$ at 1100 K and $2.8\times10^{-18}\ \mathrm{cm^2}$ at 2000 K.[13] Light from the ArF excimer laser at 193 nm (or KrF excimer laser at 248 nm) enters the shock tube from the quartz end plate and passes along the tube. A

pulse generator was employed to trigger the laser about 150–200 μs after the arrival of the incident shock wave at the last pressure sensor.

Before each experiment, the system was pumped below 5.0×10^{-7} Torr. The temperature (T_5), density (ρ_5), and pressure (P_5) in the reflected shock regime were calculated from measured velocity of the incident shock, the composition of the test gas, the initial pressure, and the temperature using the ideal shock-wave theory[14] with Mirels' boundary layer corrections.[15,16]

We calibrated the concentration of O atoms in the shock tube with pyrolysis of N_2O, assuming a 100% yield of O atoms.[17] The concentration of O atoms is fitted with the equation

$$[\mathrm{O}]/10^{13}\ \text{molecule cm}^{-3} = 4.4233A - 0.0336A^2 + 2.5741A^3 \quad (3)$$

in which absorbance A is calculated with the equation

$$A = \ln(I_0/I) \quad (4)$$

in which the light intensity before and after production of O atoms is denoted as I_0 and I, respectively.

He (99.9995%, AGA Specialty Gases), Ar (99.9995%, AGA Specialty Gases), N_2O (99%, Scott Specialty Gases), O_2 (99.999%, Scott Specialty Gases), and SO_2 (99.98%, Matheson) were used without further purification. CH_3OH (99.9%, Mallinckrodt, Analytical Reagent grade) was purified by passing the vapor though P_2O_5 to remove trace water impurity. Mixtures of CH_3OH in Ar (100–500 ppm) and SO_2 in Ar (100–900 ppm) were used.

III. COMPUTATIONAL METHODS

The geometry of reactants, transition states, and products of the $O+CH_3OH$ system was optimized at the Becke-3-Lee–Yang–Parr (B3LYP)/6−311+$G(3df,2p)$ level of theory with Becke's three-parameter nonlocal exchange functional[18] and the nonlocal correlation functional of Lee *et al.*[19] Single-point energies of all species were calculated with the coupled cluster singles, doubles (triples) [CCSD(T)]/6−311+$G(3df,2p)$ method,[20] based on the optimized geometries at the B3LYP/6−311+$G(3df,2p)$ level.

The rate coefficients were calculated with conventional transition state theory (TST), canonical variational transition (CVT) state theory with zero curvature tunneling (ZCT) corrections, and small curvature tunneling (SCT) corrections using the POLYRATE program of Corchado *et al.*[21]

All calculations were carried out with GAUSSIAN 03 (Ref. 22) programs using a personal computer (PC) cluster and the computers at the Emerson Computation Center of Emory University.

IV. RESULTS AND DISCUSSION

A. Rate coefficient k_1 for $O+CH_3OH$

The experiments were carried out under pseudo-first-order conditions with $[CH_3OH]_0 \gg [O]$. Figure 2 shows a typical temporal profile recorded for the mixture containing SO_2, CH_3OH, and Ar after laser photolysis at 193 nm. The

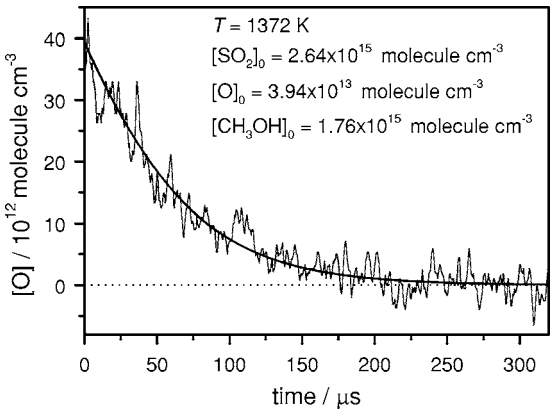

FIG. 2. A typical temporal profile of [O] observed after irradiation of a sample containing SO_2 (300 ppm) and CH_3OH (200 ppm) in Ar. T = 1372 K and total density = 8.79×10^{18} molecule cm^{-3}. The thick solid line represents the fitted results using the model described in text.

concentration of O atoms at reaction period t $[O]_t$ is derived according to Eqs. (3) and (4). $[O]_t$ follows an exponential decay in the initial stage. The apparent pseudo-first-order rate coefficient k^I is derived with the equation

$$\ln([\mathrm{O}]_t/[\mathrm{O}]_0) = -k^I t + at^2 - bt^3 \quad (5)$$

in which t is the reaction time and a and b are the fitting parameters to account for deviation from the exponential decay due to secondary reactions. The apparent bimolecular rate coefficient, k_1' is thus derived from

$$k_1' = k^I/[\mathrm{CH_3OH}]_0. \quad (6)$$

Comparison of k_1' with the true bimolecular rate coefficient k_1 provides information on the extent of interference due to secondary reactions.

At low temperature, previously observed deuterium isotopic effects on rate coefficients indicate that reaction (1) is dominated by channel (1a). Grotheer and Just[6] observed similar apparent decay rates for reactions of $O+CH_3OH$ and $O+CH_3OD$ at 305 K, which are ~8 times greater than those of $O+CD_3OH$ and $O+CD_3OD$, indicating that the main reaction channel is the abstraction of the H atom of the methyl group. However, as temperature increases, reaction (1b) may become important. Our theoretical calculations (discussed in Sec. IV C) show that reaction (1c) is unimportant under our experimental conditions and the branching ratio of reaction (1b) increases from ~0.13 at 300 K to ~0.5 at 1700 K. Because we are only probing the decay of [O] and cannot distinguish between channels (1a) and (1b), we employed branching ratios calculated theoretically in this work in the model to derive the total decay coefficient.

Photolysis of SO_2 at 193 nm is more efficient in generating O atoms, thus enabling us to use smaller concentrations of SO_2. However, irradiation of CH_3OH with light at 193 nm produces CH_3O and H.[23] The effect of CH_3O production on the decay of [O] was examined by employing the photolysis laser at 248 nm, at which wavelength photolysis of CH_3OH is negligible. We estimate the photolysis yield by the following equation:

$$[CH_3O]_0 = \sigma F [CH_3OH] \phi \tag{7}$$

in which σ is the cross section (cm^2 $molecule^{-1}$) of CH_3OH,[24] F is the fluence (photons cm^{-2}) of the laser, and ϕ is the photolysis yield.[23] No significant variations in derived rate coefficients were observed for photolysis of SO_2 at 193 and 248 nm.

Several interference reactions need to be considered. At high temperatures, pyrolysis of CH_3OH is non-negligible.[10] According to modeling, at 1777 K and $[CH_3OH]_0 = 5.95 \times 10^{14}$, $[SO_2]_0 = 2.95 \times 10^{15}$, and $[Ar] = 5.91 \times 10^{18}$ molecule cm^{-3}, about one-half of CH_3OH decomposes within 90 μs.

$$CH_3OH(+M) \rightarrow CH_3 + OH(+M) \tag{8a}$$

$$\rightarrow CH_2OH + H(+M). \tag{8b}$$

The products CH_2OH and CH_3 react rapidly with O atoms

$$O + CH_2OH \rightarrow H_2CO + OH, \tag{9}$$

$$O + CH_3 \rightarrow H_2CO + H. \tag{10}$$

Hence, subsequent reactions involving H and OH need to be considered.

Because we used SO_2 as the source of O atoms, reactions involving SO, SO_2, and SO_3 should also be considered.

$$O + SO \rightarrow S + O_2, \tag{11a}$$

$$O + SO(+M) \rightarrow SO_2(+M), \tag{11b}$$

$$O + SO_2(+M) \rightarrow SO_3(+M), \tag{12a}$$

$$O + SO_2 \rightarrow SO + O_2. \tag{12b}$$

We modeled observed temporal profiles of [O] with a commercial kinetic modeling program FACSIMILE.[25] The model employed is listed in Table II; it is basically a simplified version of that employed by Held and Dryer[1] with additional reactions involving S, SO_x, and CH_3. The rate coefficients are obtained from the literature unless noted. It should be noted that the inclusion of 50 reactions or so in the model is only for completeness. If we use a simplified model with ten reactions, the results are within 15% of those derived with a more complete model.

Because the laser was triggered about 50–100 μs after arrival of the reflected shock wave at the observation zone, pyrolysis of CH_3OH before generation of O atoms should be taken into account, especially at high temperature. We modeled these reactions in two separate periods: the first period started from the arrival of the reflected shock wave and ended with the arrival of the photolysis laser pulse, and the second period started on arrival of the photolysis laser pulse. In the first period, we used [O]=0 to derive concentrations of all reactants and intermediates at the end of this period, which were then employed in the second period, along with experimentally observed concentration of laser-produced O atoms, to model the temporal profile of [O]. In the fitting, the branching ratio of the title reaction calculated quantum chemically in this work and the literature values of rate coefficients of all reactions except the title reaction k_1 were held constant, and the bimolecular rate coefficient k_1 was varied to yield the best fit.

The experimental conditions and values of k_1 for 44 measurements in a temperature range of 835–1777 K using mixtures of various concentrations of CH_3OH and SO_2 are summarized in Table III. We list k_1'/k_1 in Table III for comparison; except for a few cases under extreme conditions, most values of k_1' obtained with Eq. (6) from pseudo-first-order decays are within 25% of k_1, indicating that even a pseudo-first-order model is adequate in these cases. However, for data at high temperature and high concentration of SO_2, k_1' is greater than k_1 by factors as much as 2.4, indicating that interference reactions are non-negligible.

Sensitivity analysis shows that rate coefficient of the title reaction is most sensitive to variations of rate coefficients of reactions (12a) and (32) at low temperatures and reactions (8a), (10), (27), (28a), (32), (33), and (50), at high temperatures. In most cases at temperatures below 1550 K, the rate coefficient k_1 varies by less than 20% if one of the above reactions was neglected. In the extreme case at temperature near 1770 K at which pyrolysis of CH_3OH becomes important, we found that the rate coefficient k_1 would increase by as much as 2.7 times if k_{10} was neglected in the model and k_1 would decrease by a similar factor if k_{27} was neglected in the model.

Some representative decay curves covering the whole temperature range of study were also modeled with a complete model consisting of 89 reactions employed by Held and Dryer,[1] eight reactions involving sulfur compounds and eight additional reactions [reactions (26b), (27), (28a), (28b), (29b), (35b), (48b), and (50)] not included in the model of Held and Dryer.[1] The derived rate coefficients are similar to those listed in Table III using our model, with deviations less than 18%.

We tested the effect of branching ratio $k_{1a}/(k_{1a}+k_{1b})$ on the derived total rate coefficient k_1 and found that the derived rate coefficient k_1 is insensitive to the branching ratio at all temperatures. Presumably this is because secondary reactions associated with CH_3O and CH_2OH have similar effects on the decay of O atoms. We also tested the effect of pyrolysis of CH_3OH before its reaction with O atoms. Pyrolysis of CH_3OH has two counteractive effects: the decrease in $[CH_3OH]$ and effects due to secondary reactions involving pyrolysis products CH_3, OH, CH_2OH, and H. At temperatures below 1650 K, when we took out the simulation of the first period (i.e., to assume that pyrolysis of CH_3OH was negligible before the photolysis laser arrived), we found that the fitted rate coefficients k_1 increased by $<20\%$, indicating that the effect of $\sim 10\%$ decrease in $[CH_3OH]$ during the first period was smaller than the effect due to secondary reactions. In contrast, we found that k_1 decreased by $<15\%$ for temperatures above 1700 K because 20%–40% of CH_3OH dissociated in the first period.

The values of k_1 at various temperatures are compared with the previous reports in Figs. 1 and 3. Our rate coefficients correlate well with the data of KSTKM (Ref. 5) and GJ (Ref. 6) in the overlapped range of temperatures. Our

TABLE II. Reaction models employed to derive rate coefficients of $O+CH_3OH$.

No.	Reaction	Rate expression	Ref.
1a	$O+CH_3OH \rightarrow OH+CH_2OH$	fitted	
1b	$O+CH_3OH \rightarrow OH+CH_3O$	k_{1b}/k_{1a} calculated from theory	
8a	$CH_3OH(+M) \rightarrow CH_3+OH(+M)$	$k_\infty: 1.9\times10^{16}\exp[-(46\,140/T)]$ $k_0: 4.9\times10^{20}T^{-7.35}\exp[-(48\,017/T)]$	10[a,b]
8b	$CH_3OH(+M) \rightarrow CH_2OH+H(+M)$	$k_\infty: 2.96\times10^{16}T^{-0.08}\exp[-(49\,768/T)]$ $k_0: 3.89\times10^{16}T^{-6.33}\exp[-(51\,860/T)]$	10[a,c]
9	$CH_2OH+O \rightarrow H_2CO+OH$	7.0×10^{-11}	10
10	$CH_3+O \rightarrow H_2CO+H$	1.41×10^{-10}	27
11a	$O+SO \rightarrow S+O_2$	$3.0\times10^{-11}\exp[-(6980/T)]$	28
11b	$O+SO(+M) \rightarrow SO_2(+M)$	$3.3\times10^{-26}T^{-1.84}$	29
12a	$O+SO_2(+M) \rightarrow SO_3(+M)$	$1.21\times10^{-33}\exp(3136/T)$	30
12b	$O+SO_2 \rightarrow O_2+SO$	$8.3\times10^{-12}\exp[-(9800/T)]$	31
21	$SO(+M) \rightarrow S+O(+M)$	$6.61\times10^{-10}\exp[-(53\,885/T)]$	32
22	$S+O_2 \rightarrow SO+O$	$9.02\times10^{-19}T^{2.11}\exp(730/T)$	33
23	$O+SO_3 \rightarrow O_2+SO_2$	$2.19\times10^{-12}\exp[-(3070/T)]$	30
24	$O+O(+M) \rightarrow O_2(+M)$	$5.21\times10^{-35}\exp(900/T)$	34
25	$CH_3+O_2 \rightarrow CH_3O+O$	$4.9\rightarrow10^{-11}\exp[-(15\,340/T)]$	35
26a	$CH_3+CH_3(+M) \rightarrow C_2H_6(+M)$	$k_\infty: 1.5\times10^{-7}T^{-1.18}\exp[-(329/T)]$ $k_0: 8.77\times10^{-7}T^{-7.03}\exp[-(1389/T)]$	36[a,d]
26b	$CH_3+CH_3 \rightarrow C_2H_5+H$	$5.25\times10^{-11}\exp(-7384/T)$	37
27	$CH_3+H(+M) \rightarrow CH_4(+M)$	$k_\infty: 2.31\times10^{-8}T^{-0.534}\exp[-(270/T)]$ $k_0: 7.23\times10^{-15}T^{-4.76}\exp[-(1227/T)]$	38[a,e]
28a	$CH_3+OH \rightarrow CH_2OH+H$	3.16×10^{-11}	39
28b	$CH_3+OH \rightarrow CH_3O+H$	$3.32\times10^{-8}\exp[-(13\,800/T)]$	27
29a	$CH_3+CH_3OH \rightarrow CH_4+CH_2OH$	$5.29\times10^{-23}T^{3.2}\exp[-(3609/T)]$	10
29b	$CH_3+CH_3OH \rightarrow CH_4+CH_3O$	$2.39\times10^{-23}T^{3.1}\exp[-(3490/T)]$	10
30a	$HCO+O \rightarrow CO+OH$	5×10^{-11}	40
30b	$HCO+O \rightarrow CO_2+H$	5×10^{-11}	40
31	$HCO(+M) \rightarrow H+CO(+M)$	$1.15\times10^{-6}T^{-1}\exp[-(8550/T)]$	41
32	$H_2CO+O \rightarrow HCO+OH$	$3.0\times10^{-11}\exp[-(1552/T)]$	42
33	$H_2CO+OH \rightarrow HCO+H_2O$	$6.47\times10^{-11}\exp[-(705/T)]$	43
34	$H_2CO+H \rightarrow HCO+H_2$	$3.62\times10^{-16}T^{1.77}\exp[-(1509/T)]$	44
35a	$CH_3O+O \rightarrow H_2CO+OH$	1.0×10^{-11}	34
35b	$CH_3O+O \rightarrow CH_3+O_2$	$3.55\times10^{-11}\exp[-(239/T)]$	45
36	$CH_3O+OH \rightarrow H_2CO+H_2O$	3×10^{-11}	34
37	$CH_3O+H \rightarrow H_2CO+H_2$	3×10^{-11}	40
38	$CH_3O+CH_3O \rightarrow CH_3OH+H_2CO$	1×10^{-10}	34
39	$CH_3O+HCO \rightarrow CH_3OH+CO$	1.5×10^{-10}	34
40	$CH_3O(+M) \rightarrow H_2CO+H(+M)$	$9.04\times10^{-11}\exp[-(6794/T)]$	46
41	$CH_2OH+OH \rightarrow H_2CO+H_2O$	4×10^{-11}	10
42a	$CH_2OH+H \rightarrow CH_3+OH$	1.6×10^{-10}	10
42b	$CH_2OH+H \rightarrow H_2CO+H_2$	1.66×10^{-11}	47
43	$CH_2OH(+M) \rightarrow H_2CO+H(+M)$	$k_\infty: 2.8\times10^{14}T^{-0.73}\exp[-(16\,509/T)]$ $k_0: 9.98\times10^{9}T^{-5.39}\exp[-(18\,209/T)]$	10[a,f]
44a	$CH_2OH+CH_2OH \rightarrow HOCH_2CH_2OH$	1.6×10^{-11}	10
44b	$CH_2OH+CH_2OH \rightarrow CH_3OH+H_2CO$	8×10^{-12}	10
45	$CH_2OH+CH_3O \rightarrow CH_3OH+H_2CO$	4×10^{-11}	10
46a	$CH_2OH+HCO \rightarrow CH_3OH+CO$	2×10^{-10}	10
46b	$CH_2OH+HCO \rightarrow H_2CO$	3×10^{-10}	10
47a	$CH_3OH+OH \rightarrow CH_2OH+H_2O$	$2.39\times10^{-18}T^{2}\exp(423/T)$	48
47b	$CH_3OH+OH \rightarrow CH_3O+H_2O$	$1.66\times10^{-11}\exp[-(854/T)]$	49
48a	$CH_3OH+H \rightarrow CH_2OH+H_2$	$2.72\times10^{-17}T^{2}\exp[-(2273/T)]$	48
48b	$CH_3OH+H \rightarrow CH_3+H_2O$	$3.32\times10^{-12}\exp[-(2670/T)]$	50
48c	$CH_3OH+H \rightarrow CH_3O+H_2$	$6.64\times10^{-11}\exp[-(3067/T)]$	49
49	$CH_3OH+CH_3O \rightarrow CH_2OH+CH_3OH$	$5\times10^{-13}\exp[-(2050/T)]$	10
50	$OH+O \rightarrow H+O_2$	$2.3\times10^{-11}\exp(110/T)$	51
51	$O+H_2O \rightarrow 2OH$	$9.21\times10^{-11}\exp[-(9611/T)]$	52

[a] k_0 and k_∞ refer to low- and high-pressure limits, respectively. The F_c parameters in the Troe equation are listed separately. Unless otherwise noted, all species are assumed to have a third body efficiency of 1.0.
[b] $F_c=(1-0.414)\exp[-(T/279)]+0.414\exp[-(T/5459)]$.
[c] $F_c=(1-0.773)\exp[-(T/693)]+0.773\exp[-(T/5333)]$.
[d] $F_c=(1-0.619)\exp[-(T/73.2)]+0.619\exp[-(T/1180)]$. Enhanced third body coefficient (relative to N_2): $\eta_{Ar}=0.7$.
[e] $F_c=(1-0.783)\exp[-(T/74)]+0.783\exp[-(T/2941)]+\exp[-(6964/T)]$. Enhanced third body coefficient (relative to N_2): $\eta_{Ar}=0.7$.
[f] $F_c=(1-0.96)\exp[-(T/67.6)]+0.96\exp[-(T/1855)]+\exp[-(7543/T)]$.

TABLE III. Experimental conditions and rate coefficients k_1 for the reaction $O+CH_3OH$. (P_1: pressure of reactant gas mixture; P_4: pressure of driver gas; M_s: Mach number; T_5: temperature of reaction. Concentrations are in units of molecule cm^{-3}; k_1 in cm^3 molecule^{-1} s^{-1} are fitted with kinetic modeling and k_1' are derived from pseudo-first-order decays; see text.)

P_1 (Torr)	P_4 (Torr)	M_s	T_5 (K)	$[SO_2]$ (10^{15})	$[O]$ (10^{13})	$[CH_3OH]$ (10^{14})	k_1 (10^{-12})	k_1'/k_1
			SO_2 (302 ppm)+CH_3OH (102 ppm), 193 nm					
60.1	2000	2.26	1279	2.99	3.90	10.05	8.43±0.18	1.12
51.1	2000	2.37	1393	2.68	3.46	9.01	12.20±0.26	1.09
45.4	2000	2.46	1485	2.47	2.99	8.30	14.02±0.38	1.09
35.3	2000	2.60	1646	2.03	2.27	6.81	15.78±0.86	2.05
31.1	2000	2.65	1713	1.82	2.28	6.12	18.95±1.40	2.30
30.1	2000	2.70	1766	1.79	2.07	6.01	23.96±2.25	2.12
			SO_2 (500 ppm)+CH_3OH (101 ppm), 193 nm					
79.1	2000	2.12	1138	6.01	9.04	12.13	5.52±0.11	1.00
65.1	2000	2.22	1234	5.22	9.28	10.54	8.96±0.15	0.98
50.0	2000	2.38	1404	4.34	7.01	8.77	11.05±0.20	1.09
45.1	2000	2.44	1468	4.02	6.28	8.11	14.14±0.26	0.98
36.0	2000	2.59	1638	3.40	4.55	6.86	16.19±0.55	1.34
35.1	2000	2.59	1640	3.32	5.00	6.70	19.47±0.55	1.64
30.0	2000	2.71	1777	2.95	3.29	5.95	25.55±1.69	2.05
			SO_2 (208 ppm)+CH_3OH (151 ppm), 193 nm					
91.3	2000	2.05	1075	2.77	4.21	20.06	5.07±0.11	1.06
80.1	2000	2.07	1092	2.45	3.70	17.80	4.88±0.15	0.98
80.4	2000	2.11	1128	2.52	3.58	18.28	5.47±0.13	1.12
60.3	1800	2.17	1188	1.96	2.62	14.21	6.78±0.26	1.04
70.2	2000	2.20	1212	2.31	3.33	16.78	7.60±0.18	1.05
			SO_2 (300 ppm)+CH_3OH (200 ppm), 193 nm					
121.0	2000	1.93	965	4.88	8.50	32.50	3.53±0.08	1.24
80.0	2000	2.13	1145	3.67	5.87	24.44	5.61±0.09	1.27
65.0	2000	2.23	1246	3.15	5.23	21.01	8.17±0.16	0.99
51.2	2000	2.35	1372	2.64	3.94	17.57	8.69±0.17	1.10
40.2	2000	2.51	1550	2.22	3.46	14.78	14.42±0.48	1.39
35.0	2000	2.60	1649	1.99	2.79	13.29	16.60±0.90	1.61
			SO_2 (100 ppm)+CH_3OH (300 ppm), 193 nm					
190.2	2000	1.78	835	2.28	3.95	67.95	1.60±0.09	1.31
140.2	2000	1.85	893	1.78	5.56	53.11	2.19±0.05	1.33
113.9	2000	1.96	991	1.58	3.61	47.00	3.03±0.10	1.07
111.1	2000	1.97	995	1.54	3.56	46.01	3.26±0.08	1.05
80.5	2000	2.12	1139	1.23	3.30	36.840	4.94±0.11	0.94
60.0	2000	2.28	1295	1.00	2.75	29.89	8.25±0.20	1.14
50.8	2000	2.42	1446	0.91	1.79	27.03	11.89±0.57	1.24
40.1	2000	2.53	1566	0.75	1.50	22.29	16.38±0.91	1.08
			SO_2 (101 ppm)+CH_3OH (500 ppm), 193 nm					
160.1	2000	1.80	849	1.96	4.35	96.51	1.67±0.07	0.98
120.1	2000	1.93	963	1.63	4.66	80.51	3.08±0.07	1.23
100.0	2000	2.02	1039	1.44	3.31	71.17	3.32±0.09	1.06
81.4	2000	2.10	1122	1.24	3.20	61.29	4.66±0.12	1.19
			SO_2 (900 ppm)+CH_3OH (136 ppm), 248 nm					
60.2	2000	2.27	1284	8.93	2.71	13.53	7.73±0.36	1.28
50.0	2000	2.30	1315	7.53	1.97	11.40	9.30±0.45	1.13
50.3	2000	2.37	1393	7.84	2.91	11.88	9.54±0.35	1.21
45.3	2000	2.43	1455	7.24	2.08	10.97	10.37±0.64	1.25
41.0	2000	2.48	1513	6.70	2.76	10.14	12.18±0.59	1.24
35.3	2000	2.59	1641	6.02	2.83	9.12	18.11±1.41	1.82
30.3	2000	2.70	1766	5.36	3.18	8.11	23.87±3.83	2.40
30.3	2000	2.71	1775	5.37	2.10	8.13	27.15±3.97	1.63

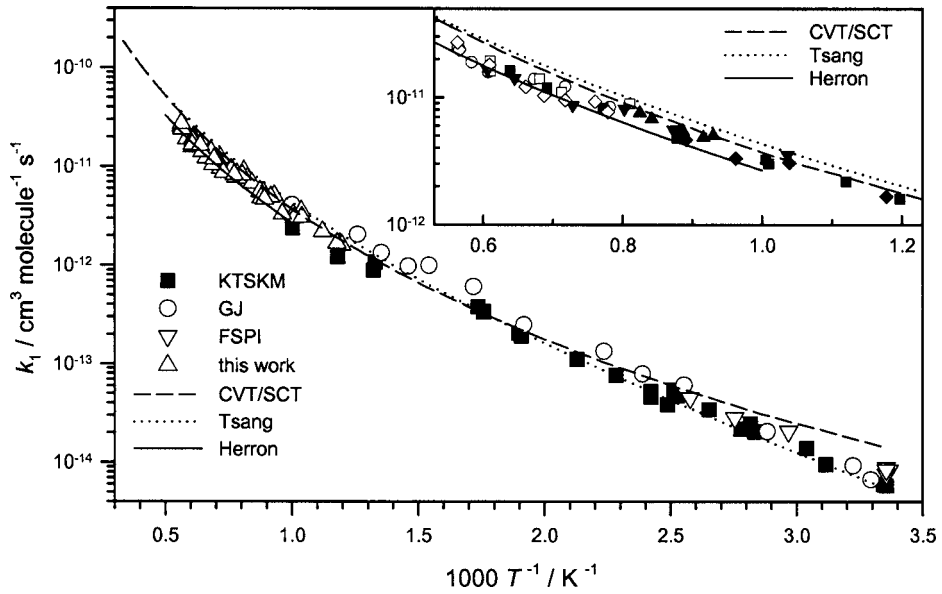

FIG. 3. Comparison of the total rate coefficient k_1 predicted with the theoretical calculations (CVT/SCT, dashed line) with the experimental results of this work (△), KTSKM (■) (Ref. 5), GJ (○) (Ref. 6), and FSPI (▽) (Ref. 7), and recommendation from Tsang (dotted line) (Ref. 10) and Herron (solid line) (Ref. 26). Insert: expanded view of our experimental and calculation results. ○: SO_2(302 ppm)+CH_3OH(102 ppm); □: SO_2(500 ppm)+CH_3OH(101 ppm); ▲: SO_2(208 ppm)+CH_3OH(151 ppm); ▼: SO_2(300 ppm)+CH_3OH(200 ppm); ■: SO_2(100 ppm)+CH_3OH(300 ppm); ◆: SO_2(101 ppm)+CH_3OH(500 ppm); ◇: SO_2(900 ppm)+CH_3OH(136 ppm), irradiation at 248 nm. Unless otherwise specified, photolysis wavelength is 193 nm.

work extends the temperature range of study from 1006 to 1777 K. Fitting our results to an Arrhenius equation yields

$$k_1 = (2.29 \pm 0.18) \times 10^{-10} \times \exp[-(4210 \pm 100)/T] \text{ cm}^3 \text{ molecule}^{-1} \text{ s}^{-1} \quad (13)$$

for $835 < T/\text{K} < 1777$, in which the listed errors represent one standard deviation in fitting, unless otherwise noted. The observed value of $E_a/R = 4210$ K is much greater than the values $E_a/R = 2530-2750$ K reported previously from measurements below 1000 K,[5,6] indicating clearly the non-Arrhenius temperature dependence with an upward curvature. Fitting our data combined with the previous results of KTSKM (Ref. 5) yields the expression

$$k_1 = (2.74 \pm 0.07) \times 10^{-18} T^{2.25\pm0.13} \times \exp[-(1500 \pm 90)/T] \text{ cm}^3 \text{ molecule}^{-1} \text{ s}^{-1} \quad (14)$$

for $298 \leqslant T/\text{K} \leqslant 1777$.

B. Potential-energy surfaces and reaction mechanism

Geometries of the molecular reactant (CH_3OH), transition states (TS1, TS2, and TS3), and products (OH, HO_2, CH_3, CH_2OH, and CH_3O) optimized at the B3LYP/6-311 $+G(3df,2p)$ level are shown in Fig. 4. The potential-energy diagram obtained by the CCSD(T)/6-311$+G(3df,2p)$ single-point calculations based on the optimized geometries at the B3LYP/6-311$+G(3df,2p)$ level is presented in Fig. 5. The total energies of the reactants and relative energies of the transition states and products are listed in Table IV and the vibrational frequencies and moments of inertia of all species are summarized in Table V.

The oxygen atom may attack CH_3OH at one of the H atoms of the methyl group [reaction (1a)], the H atom of the hydroxyl group [reaction (1b)], or the O atom of the hydroxyl group [reaction (1c)]. As shown in Fig. 5, reaction (1a) proceeds via TS1 with a barrier of 6.3 kcal mol^{-1} and forms CH_2OH and OH with energy of −5.5 kcal mol^{-1} relative to that of the reactants. Reaction (1b) proceeds via TS2 with a barrier of 10.6 kcal mol^{-1} and forms CH_3O and OH with energy of 2.4 kcal mol^{-1} above that of the reactants. Reaction (1c) proceeds via TS3 with a barrier of 52.7 kcal mol^{-1}, giving CH_3 and HO_2 with energy of 28.1 kcal mol^{-1} above that of the reactants; the contribution of this channel to the rate coefficient is hence negligible in the temperature range of our study. The predicted enthalpies of reaction for the three branching reactions are compared with the experimental values in Table IV. The agreement between theory and experiment is satisfactory.

As shown in Fig. 4, the reacting atoms O, H, and C in TS1 are almost linear with ∠OHC=177°; the length of the breaking C–H bond increases by 0.12 Å from that of CH_3OH. The imaginary vibrational wave number of TS1 is $426i$ cm^{-1}. For TS2, ∠OHO=161° and the C–H bond length increases by 0.15 Å from that of CH_3OH. The imaginary vibrational wave number of TS2 is $1313i$ cm^{-1}. The significant difference between the two imaginary frequencies may be conceived by comparing the lengths of the forming O–H and the breaking C–H bonds in TS1 and TS2, as illustrated in Fig. 4. For TS3, the O–O bond length is 1.574 Å and the C–O bond is 1.987 Å; both are longer than those of HOO and CH_3OH. The imaginary vibrational wave number of TS3 is $942i$ cm^{-1}.

C. Calculation and comparison of rate coefficients

The rate coefficients of reactions (1a) and (1b) calculated with TST, CVT, CVT/ZCT, and CVT/SCT methods in the temperature range of 300–3000 K are presented in Fig. 6. As

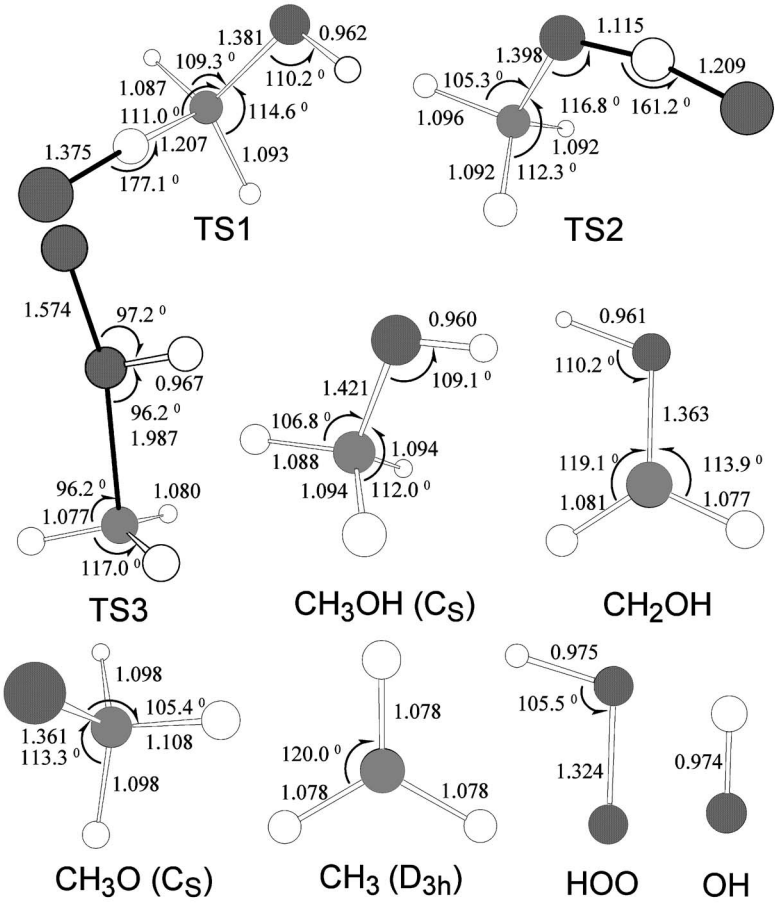

FIG. 4. Geometries of reactant CH_3OH, three transition states (TS1, TS2, and TS3) and products OH, HO_2, CH_3, CH_2OH, and CH_3O of the $O+CH_3OH$ system optimized at the B3LYP/6-311+$G(3df,2p)$ level. Listed bond lengths are in angstrom and bond angles are in degree.

shown in panels (A) and (B) of Fig. 6, the rate coefficients of reactions (1a) and (1b) predicted with TST are similar to those predicted with CVT because of their moderately high barriers. The rate coefficients predicted with CVT/ZCT are smaller than those predicted with CVT/SCT. At 300 K, the rate coefficients of reactions (1a) and (1b) predicted with CVT/SCT are 24 and 10 500 times that predicted with CVT, respectively.

The branching ratio of channels (1a) and (1b) predicted with the CVT/SCT method for 300–3000 K are plotted in Fig. 6(c). Reaction (1a) is the major channel at low temperatures; its branching ratio decreases from 0.87 at 300 K to 0.50 at 1700 K. Above 1700 K, reaction (1b) becomes the major channel; its branching ratio increases from 0.50 at 1700 K to 0.62 at 3000 K.

In order to compare the predicted rate coefficients with the experimental data quantitatively, we fit the rate coefficients predicted with CVT/SCT in the temperature range of 300–1000 K to the Arrhenius form to yield

$$k_{1a}(T) = 1.77 \times 10^{-11} \times \exp[-(2298/T)]\ \mathrm{cm^3\ molecule^{-1}\ s^{-1}}, \qquad (15)$$

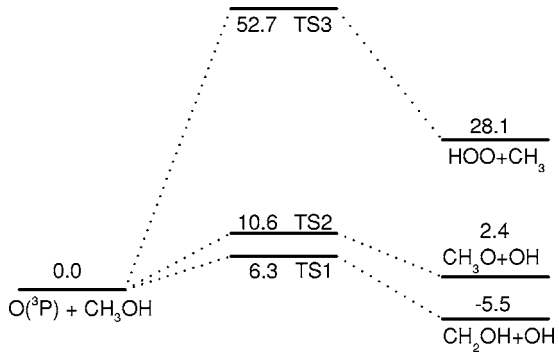

FIG. 5. Potential-energy diagram for various channels of the reaction $O+CH_3OH$ based on energies calculated with CCSD(T)/6-311+$G(3df,2p)$//B3LYP/6-311+$G(3df,2p)$. The listed energies are in kcal mol^{-1}.

TABLE IV. Total and relative energies (total energies are in a.u. and relative energies are in kcal mol^{-1}) of reactants, transition states, and products of the reaction $O+CH_3OH$.

Species or reactions	zero-point energy	B3LYP/ 6-311+$G(3df,2p)$	CCSD(T)[a]/ 6-311+$G(3df,2p)$	ΔH_{expt}[b]
$O+CH_3OH$	0.0511	−190.864 006	−190.468 6391	
TS1	−2.3	−1.2	6.3	
TS2	−4.7	3.4	10.6	
TS3	−2.4	44.7	52.7	
CH_2OH+OH	−3.5	−7.7	−5.5	−6.8±0.8
CH_3O+OH	−4.1	−0.5	2.4	1.2±1.1
HO_2+CH_3	−4.5	24.1	28.1	26.3±0.9

[a]Based on optimized geometries calculated at B3LYP/6-311+$G(3df,2p)$.
[b]At 0 K, ΔH_f (in kcal mol^{-1}) are as follows: O, 58.98 (Ref. 53); CH_3OH, 45.43 (Ref. 54); OH, 8.85±0.07 (Ref. 55); HO_2, 4.0±0.8 (Ref. 56); CH_3, 35.86±0.07 (Ref. 57); CH_2OH, −2.1±0.7 (Ref. 58); CH_3O, 5.9±1.0 (Ref. 59).

TABLE V. Vibrational wave numbers and moments of inertia I_i for the reactants, transition states, and products of the reaction $O+CH_3OH$ calculated with B3LYP/6-311+$G(3df,2p)$.

Species	I_i (a.u.)	Vibrational wave numbers (cm^{-1})
OH	0.0, 3.2, 3.2	3722
HO_2	2.9, 53.2, 56.1	1171, 1443, 3613
CH_3	6.3, 6.3, 12.5	539, 1407, 1407, 3108, 3284, 3284
CH_2OH	9.3, 60.2, 68.9	411, 528, 1054, 1204, 1356, 1483, 3130, 3272, 3851
CH_3O	11.4, 64.1, 64.5	684, 960, 1108, 1355, 1366, 1513, 2885, 2959, 3002
CH_3OH	14.0, 72.9, 75.5	288, 1043, 1077, 1174, 1366, 1481, 1500, 1511, 2991, 3038, 3107, 3856
TS1	51.5, 357.3, 392.3	137, 289, 476, 958, 1068, 1137, 1160, 1312, 1380, 1420, 1491, 3026, 3138, 3834, 426*i*
TS2	49.1, 285.7, 323.1	142, 167, 189, 616, 1030, 1129, 1150, 1235, 1427, 1435, 1506, 2985, 3043, 3070, 1313*i*
TS3	18.0, 360.8, 366.5	86, 216, 257, 427, 607, 669, 983, 1203, 1422, 1434, 3102, 3258, 3274, 3784, 942*i*

$$k_{1b}(T) = 1.50 \times 10^{-11} \times \exp[-(2845/T)]\ \mathrm{cm^3\ molecule^{-1}\ s^{-1}}. \quad (16)$$

At higher temperatures, the rate coefficients increase more rapidly with temperature. We fit the rate coefficients predicted with CVT/SCT in the temperature range of 300–3000 K with a three-parameter function to yield

$$k_{1a}(T) = 8.80 \times 10^{-20} T^{2.61} \times \exp[-(941/T)]\ \mathrm{cm^3\ molecule^{-1}\ s^{-1}}, \quad (17)$$

$$k_{1b}(T) = 4.15 \times 10^{-23} T^{3.64} \times \exp[-(974/T)]\ \mathrm{cm^3\ molecule^{-1}\ s^{-1}}. \quad (18)$$

The predicted total rate coefficients may be expressed with the three-parameter equation

$$k_1(T) = 1.93 \times 10^{-21} T^{3.20} \times \exp[-(763/T)]\ \mathrm{cm^3\ molecule^{-1}\ s^{-1}}. \quad (19)$$

The total rate coefficients predicted with CVT/SCT in the temperature range of 300–3000 K are plotted in Fig. 3 to compare with the experimental data of KTSKM,[5] GJ,[6] FSPI,[7] and this work. In general, rate coefficients predicted with CVT/SCT are in satisfactory agreement with the experimental values reported previously, indicating that the SCT method treats tunneling effects adequately. At low temperatures, the predicted rate coefficients are slightly greater than the experimental values, but within expected uncertainties of calculation and experiments. At high temperatures, the predicted rate coefficients fit satisfactorily with the experimental data of this work and of KTSKM (Ref. 5) and GJ.[6]

Our experimental data are about 20% smaller than the theoretically predicted rate coefficients, but the deviations are within expected uncertainties. The equation reported by Herron[26]

$$k_1(T) = 3.99 \times 10^{-19} T^{2.50} \times \exp[-(1550/T)]\ \mathrm{cm^3\ molecule^{-1}\ s^{-1}} \quad (20)$$

is in satisfactory agreement with our experimental results in the overlapping temperature range of 1000–1777 K. The equation reported by Tsang[10]

$$k_1(T) = 6.44 \times 10^{-19} T^{2.50} \times \exp[-(1550/T)]\ \mathrm{cm^3\ molecule^{-1}\ s^{-1}} \quad (21)$$

is slightly greater than our experimental results but appears to fit well with the calculated rate coefficients at high temperatures, as illustrated in Fig. 3.

V. CONCLUSION

The total rate coefficients of the reaction $O(^3P)+CH_3OH$ in the temperature range of 835–1777 K were determined using a diaphragmless shock tube with atomic resonance absorption detection of O atoms. Our results extended the upper limit of the temperature range of study from 1006 to 1777 K and clearly indicate a non-Arrhenius behavior of the rate coefficient. The rate coefficients obtained in this work correlate well with those determined previously by Keil *et al.*;[5] they were combined to yield the temperature dependence as $k_1=(2.74\pm0.07)\times10^{-18}T^{2.25\pm0.13}\exp[-(1500\pm90)/T]\ \mathrm{cm^3\ molecule^{-1}\ s^{-1}}$ for $298 \leqslant T/\mathrm{K} \leqslant 1777$. The theoretical calculations at the CCSD(T)/6-311+$G(3df,2p)$//B3LYP/6-311+$G(3df,2p)$ level predict transition states and barriers for various channels. The rate coefficients predicted with CVT/SCT show that branching ratios of two accessible reaction channels to form $OH+CH_2OH$ (1a) and $OH+CH_3O$ (1b) vary with temperature. At 300 K, reaction (1a) dominates, whereas above 1700 K, reaction (1b) becomes more important. The predicted total rate coefficients are in satisfactory agreement with our experimental data at high temperature (835–1777 K) and those reported by Keil *et al.*[5] at 298–998 K.

ACKNOWLEDGMENTS

One of the authors (Y.P.L.) thanks the National Science Council of Taiwan (Grant No. NSC93-2119-M-009-002) for support. The authors (M.C.L., S.C.X., and Z.F.X.) thank the support from the Basic Energy Science, Department of Energy, under Contract No. DE-FG02-97-ER14784, and Cherry L. Emerson Center for Scientific Computation of Emory

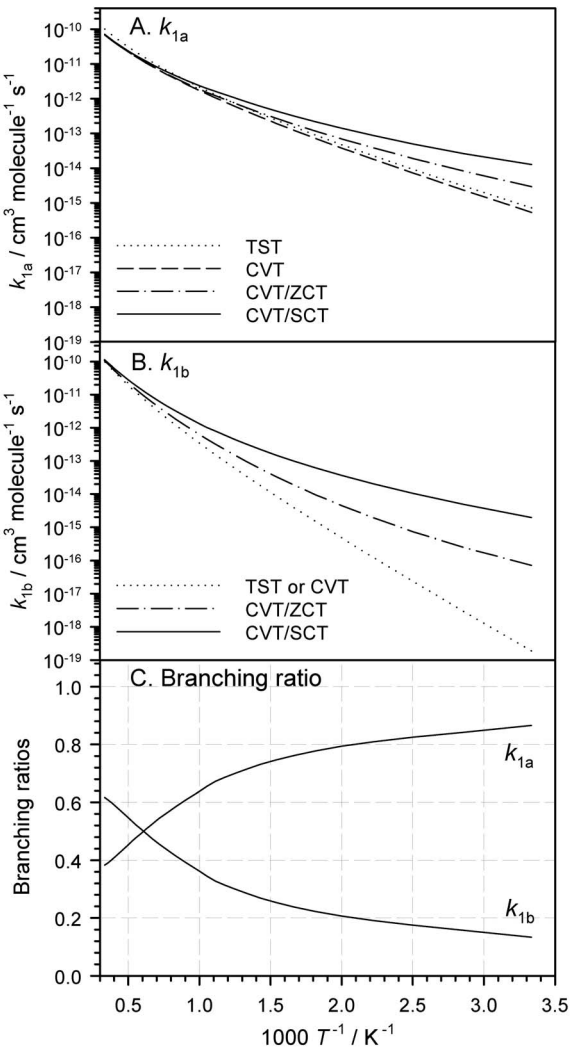

FIG. 6. Theoretically predicted rate coefficients for the reaction O $+CH_3OH$ in the temperature range of 300–3000 K. Solid line: CVT with SCT tunneling correction; dotted line: TST; dashed line: CVT; dot-dashed line: CVT with ZCT tunneling correction. (A) k_{1a}, (B) k_{1b}, and (C) branching ratios for reactions (1a) and (1b).

University for the use of its resources, which are in part supported by a National Science Foundation Grant (Grant No. CHE-0079627) and an IBM Shared University Research Award. Another author (M.C.L.) also acknowledges the support from the National Science Council of Taiwan for a Distinguished Visiting Professorship at the National Chiao Tung University in Hsinchu, Taiwan. One of the authors (S.C.X.) also thanks the support from Cherry L. Emerson Center for Scientific Computation of Emory University for a Cherry L. Emerson Visiting Fellowship.

[1] T. J. Held and F. L. Dryer, Int. J. Chem. Kinet. **30**, 805 (1998).
[2] H. F. LeFevre, J. F. Meagher, and R. B. Timmons, Int. J. Chem. Kinet. **4**, 103 (1972).
[3] V. Y. Basevich, S. M. Kogarko, and G. A. Furman, Bull. Acad. Sci. USSR, Div. Chem. Sci. Engl. Transl. 948 (1975); Izv. Akad. Nauk. SSR, Ser. Khi. 1035 (1975).
[4] C. M. Owens and J. M. Roscoe, Can. J. Chem. **54**, 984 (1976).
[5] D. G. Keil, T. Tanzawa, E. G. Skolnik, R. B. Klemm, and J. V. Michael, J. Chem. Phys. **75**, 2693 (1981).
[6] H. H. Grotheer and Th. Just, Chem. Phys. Lett. **78**, 71 (1981).
[7] R. L. Failes, D. L. Singleton, G. Paraskevopoulos, and R. S. Iewin, Int. J. Chem. Kinet. **14**, 371 (1982).
[8] L. I. Avramenko, R. V. Kolesnikova, and N. L. Kuzentsova, Izv. Akad. Nauk SSSR, Otd. Khim Nauk **4**, 599 (1961).
[9] C. Lalo and C. Vermeil, J. Chim. Phys. Phys.-Chim. Biol. **77**, 131 (1980).
[10] W. Tsang, J. Phys. Chem. Ref. Data **16**, 471 (1987).
[11] M. Koshi, M. Yoshimura, K. Fukuda, H. Matsui, K. Saito, M. Watanabe, A. Imamura, and C. Chen, J. Chem. Phys. **93**, 8703 (1990).
[12] C.-C. Hsiao, Y.-P. Lee, N. S. Wang, J. H. Wang, and M. C. Lin, J. Phys. Chem. A **106**, 10231 (2002).
[13] K. Tsuchiya, K. Yokoyama, H. Matsui, M. Oya, and G. Dupre, J. Phys. Chem. **98**, 8419 (1994).
[14] E. F. Greene and J. P. Toennies, *Chemical Reactions in Shock Waves* (Academic, New York, 1964).
[15] J. V. Michael, J. Chem. Phys. **90**, 189 (1989).
[16] J. V. Michael and J. W. Sutherland, Int. J. Chem. Kinet. **18**, 409 (1986).
[17] S. K. Ross, J. W. Sutherland, S.-C. Kuo, and R. B. Klemm, J. Phys. Chem. A **101**, 1104 (1997).
[18] A. D. Becke, J. Chem. Phys. **98**, 5648 (1993); **96**, 2155 (1992); **97**, 9173 (1992).
[19] C. Lee, W. Yang, and R. G. Parr, Phys. Rev. B **37**, 785 (1988).
[20] K. Raghavachari, G. J. Trucks, J. A. Pople, and M. Head-Gordon, Chem. Phys. Lett. **157**, 479 (1989).
[21] J. C. Corchado, Y.-Y. Chuang, P. L. Fast *et al.*, POLYRATE Version 8.7, University of Minnesota, Minneapolis, MN, 2001.
[22] M. J. Frisch, G. W. Trucks, H. B. Schlegel *et al.*, GAUSSIAN 03 Revision A.7, Gaussian, Inc., Pittsburgh, PA, 2003.
[23] S. Satyapal, J. Park, R. Bersohn, and B. Katz, J. Chem. Phys. **91**, 6873 (1989).
[24] B. M. Cheng, M. Bahou, W. C. Chen, C.-H. Yu, Y.-P. Lee, and L. C. Lee, J. Chem. Phys. **117**, 1633 (2002).
[25] FACSIMILE is a computer software for modeling process and chemical reaction kinetics released by AEA technology, Oxfordshire, United Kingdom.
[26] J. T. Herron, J. Phys. Chem. Ref. Data **17**, 967 (1988).
[27] K. A. Bhaskaran, P. Frank and Th. Just, Proc. Int. Symp. Shock Tubes Waves **12**, 503 (1980).
[28] C.-W. Lu, Y.-J. Wu, Y.-P. Lee, R. S. Zhu, and M. C. Lin, J. Phys. Chem. A **107**, 11020 (2003).
[29] A. Grillo, R. Reed, and M. W. Slack, J. Chem. Phys. **70**, 1634 (1979).
[30] O. I. Smith, S. Tseregounis, and S.-N. Wang, Int. J. Chem. Kinet. **14**, 679 (1982).
[31] D. L. Singleton and R. J. Cvetanovic, J. Phys. Chem. Ref. Data **17**, 1377 (1988).
[32] H. J. Plach and J. Troe, Int. J. Chem. Kinet. **16**, 1531 (1984).
[33] C.-W. Lu, Y.-J. Wu, Y.-P. Lee, R. S. Zhu, and M. C. Lin, J. Chem. Phys. **121**, 8271 (2004).
[34] W. Tsang and R. F. Hampson, J. Phys. Chem. Ref. Data **15**, 1087 (1986).
[35] C. L. Yu, C. Wang, and M. Frenklach, J. Phys. Chem. **99**, 14377 (1995).
[36] A. F. Wagner and D. M. Wardlaw, J. Phys. Chem. **92**, 2462 (1988).
[37] K. P. Lim and J. V. Michael, Symp. Int. Combust. Proc. **25**, 713 (1994).
[38] C. T. Bowman, R. K. Hanson, D. F. Davidson *et al.*, http://www.me.berkeley.edu/gri_mech/index.html
[39] I. T. Woods and B. S. Haynes, Symp. Int. Combust. Proc. **25**, 909 (1994).
[40] D. L. Baulch, C. J. Cobos, R. A. Cox *et al.*, J. Phys. Chem. Ref. Data **21**, 411 (1992).
[41] Y. Hidaka, T. Taniguchi, T. Kamesawa, H. Masaoka, K. Inami, and H. Kawano, Int. J. Chem. Kinet. **25**, 305 (1993).
[42] A. M. Dean, R. L. Johnson, and D. C. Steiner, Combust. Flame **37**, 41 (1980).
[43] J. Vandooren and P. J. Van Tiggelen, Symp. Int. Combust. Proc. **16**, 1133 (1977).
[44] Y. Hidaka, T. Taniguchi, H. Tanaka, T. Kamesawa, K. Inami, and H. Kawano, Combust. Flame **92**, 365 (1993).
[45] C. J. Cobos and J. Troe, J. Chem. Phys. **83**, 1010 (1985).
[46] T. K. Choudhury, Y. He, and W. A. Sanders, J. Phys. Chem. **94**, 2394 (1990).
[47] P. H. Gribb, J. E. Dove, and S. Yamazaki, Combust. Flame **88**, 169 (1992).
[48] S. C. Li and F. A. Williams, Symp. Int. Combust. Proc. **26**, 1017 (1996).
[49] W. C. Gardiner, Jr., in *Combustion Chemistry*, edited by J. Warnatz (Springer, New York, 1984).
[50] Y. Hidaka, T. Oki, and H. Kawano, J. Phys. Chem. **93**, 7134 (1989).
[51] R. Atkinson, D. L. Baulch, R. A. Cox, R. F. Hampson, Jr., J. A. Kerr, M.

J. Rossi, and J. Troe, J. Phys. Chem. Ref. Data **26**, 1329 (1997).
[52] J. W. Sutherland, P. M. Patterson, and R. B. Klemm, Symp. Int. Combust. Proc. **23**, 51 (1991).
[53] M. W. Chase, Jr., C. A. Davies, J. R. Downey, Jr., D. J. Frurip, R. A. McDonald, and A. N. Syverud, J. Phys. Chem. Ref. Data Suppl. **14**, 1 (1985); see also M. W. Chase, Jr., J. Phys. Chem. Ref. Data Monogr. 9 (1998).
[54] D. D. Wagman, W. H. Evans, V. B. Parker, R. H. Schumm, I. Halow, S. M. Bailey, K. L. Churney, and R. L. Nuttall, J. Phys. Chem. Ref. Data Suppl. **11**, 2 (1982); H. M. Rosenstock, K. Draxl, B. W. Steiner, and J. T. Herron, J. Phys. Chem. Ref. Data Suppl. **6**, 1 (1977).
[55] B. Ruscic, A. F. Wagner, L. B. Harding *et al.*, J. Phys. Chem. A **106**, 2727 (2002).
[56] M. Litorja and B. Rustic, J. Electron Spectrosc. Relat. Phenom. **97**, 131 (1998).
[57] B. Rustic, M. Litorja, and R. L. Asher, J. Phys. Chem. A **103**, 8625 (1999).
[58] B. Rustic and J. Berkowitz, J. Phys. Chem. **97**, 11451 (1993).
[59] B. Rustic, E. H. Appelman, and J. Berkowitz, J. Chem. Phys. **95**, 7957 (1991).